ISSN: 2538-5887; Pathobiology Research. 2024;27(1): 27-43

Altered iron metabolism in postmortem white matter tissue of patients with multiple sclerosis

ARTICLE INFO

Article Type
Original Research

Authors

Reyhaneh Doost[1]

Yaghoub Fathollahi[1]

Mohammad Javan[1,2*]

1 Department of Physiology, Faculty of Medical Sciences, Tarbiat Modares University, Tehran, Iran.
2 Institute for Brain and Cognition, Tarbiat Modares University, Tehran, Iran.

***Corresponding author:**

Mohammad Javan

Department of Physiology, Faculty of Medical Sciences, Tarbiat Modares University, Tehran, Iran.

Email:mjavan@modares.ac.ir

ABSTRACT

Introduction: Iron is an essential element that works as a cofactor in mitochondrial respiration, neurotransmitter biosynthesis, and myelination enzymes. Several pieces of evidence reveal that iron accumulates in demyelinating lesions in patients with multiple sclerosis (MS), and its intracellular homeostasis is disrupted, which exacerbates inflammation and demyelination.

Methods: We reanalyzed a microarray human MS dataset from GEO DataSests, under accession number GSE108000. We examined differentially expressed genes involved in iron metabolism between different types of MS lesions and peri-lesional normal-appearing white matter (PL-NAWM). We used GEO2R for differential expression analysis and created volcano plots, Venn diagrams, and pie charts for data visualization using RStudio software.

Results: We identified 58 genes involved in iron metabolism within the dataset. The expression of key iron-regulating genes, responsible for iron uptake, storage, and export, including CYBRD1, STEAP3, SLC39A14, FTL, FTH1, and CP were significantly changed. We also indicated significant alterations in the iron regulatory pathways in MS lesions and the PL-NAWM. The most prominent alterations were related to the iron uptake pathway, which showed enhanced activity.

Conclusion: Significant changes in iron regulatory gene expressions across MS lesions and the PL-NAWM may lead to dysregulation in iron homeostasis. This imbalance likely contributes to neurodegenerative processes associated with MS. The modifications in the PL-NAWM can be regarded as early-disease indicators. Recognizing these molecular changes provides valuable insights for facilitating timely MS diagnosis and developing targeted therapeutic strategies.

Keywords: Multiple sclerosis; Iron metabolism; Gene expression; MS lesions; Normal-appearing white matter; Bioinformatics

INTRODUCTION

It is well known that iron plays a crucial role in many cellular functions. It acts as a cofactor for enzymes involved in oxidative metabolism, mitochondrial respiration, neurotransmitter biosynthesis, myelination, DNA repair, and cellular proliferation and differentiation (1, 2). Even though, iron is a multivalent metal, capable of switching between two forms, ferrous and ferric, acting as a double-edged sword for the cell. Ferrous iron participates in the Fenton reaction, producing free radicals which in the excessive iron condition cause oxidative stress and push the cell toward iron-dependent programmed cell death known as ferroptosis (3, 4). Thus, its homeostasis needs to be precisely tuned and the expression of proteins involved in iron uptake, storage, and release must be balanced and coordinated in the body. One of the

most important iron carriers is transferrin, which transports iron in its ferric form. Iron influx is regulated via the transferrin receptor 1 (TfR1) or other transferrin-independent transporters including divalent metal transporter 1 (DMT1), and ZRT/IRT-like protein 14 (ZIP14). Furthermore, most CNS cells express mitoferrin1/2, iron transporters into the mitochondria. Iron is stored within ferritin composed of ferritin heavy chain (FTH) and light chain (FTL) subunits, and can leave the cell in its ferrous form through the transporter ferroportin. Hepcidin binds to ferroportin, reducing iron export from the cell (5-7).

Iron balance is disrupted and lost in many neurodegenerative disorders, including multiple sclerosis (MS) leading to iron accumulation at the demyelinating lesion sites in the brain and the spinal cord (8, 9). Inflammatory processes alter iron-regulating proteins in cells and promote iron accumulation (10, 11). The expression of iron importers such as Tfr1, DMT1, and ZIP14 is increased in microglia, astrocytes, and neurons following the LPS stimulation in vitro (12). Similar results have been shown in the studies conducted on MS animal models (13, 14). They have also revealed, that under demyelination conditions, the expression of the iron exporter ferroportin decreases in neurons and microglia following an increase in hepcidin, while it increases in astrocytes. Additionally, the expression of ferroxidase proteins is reduced in microglia, whereas ferritin protein levels rise in these cells. These findings indicate due to demyelination or inflammatory cytokines, iron accumulates inside the glial cells and neurons. Accumulation of iron causes oxidative damage and promotes the inflammatory process (15-17). Ultimately, these may result in the progression of lesions and disease exacerbation (18, 19). Studies using magnetic resonance imaging (MRI) have revealed a correlation between the severity of MS and iron accumulation in the central nervous system (CNS) (20, 21). Therefore, understanding the cellular pathways involved in intralesional iron accumulation in MS can provide insights into potential therapeutic strategies and enhance diagnostic methods for better management of multiple sclerosis.

In the present study, we reanalyzed a microarray dataset to investigate how iron metabolism is affected by MS. We looked at different types of MS lesions, including chronic active rim, inactive rim, and peri-lesional normal-appearing white matter (PL-NAWM) around the lesions. By re-analyzing the differentially expressed genes (DEGs) in each type of lesion and across all MS lesions, we could identify the proteins responsible for disrupting iron homeostasis and causing its accumulation.

METHODS

Dataset selection

To reanalyze publicly available datasets concerning MS in human patients, we selected the microarray MS dataset from the National Center for Biotechnology Information (NCBI) Gene Expression Omnibus public database (GEO), GEO DataSests, under accession number GSE108000. This dataset comprises tissues isolated from the rim and peri-lesional (PL) region of chronic active and inactive MS lesions from 15 MS patients (7 samples from chronic active lesions and 8 samples from inactive lesions, both including the rim of the lesions and the normal-appearing white matter around the lesions, totaling 40 samples), as well as white matter (WM) from 10 matched non-neurological control subjects, Using laser-based microdissection. The gene expression variances were examined using Agilent Human Gene Expression 4 × 44K v2 microarrays. Detailed donor characteristics are available in the original report (22).

Initial analysis

We assigned 4 comparisons: 1. rim of MS lesions (n=15) vs. control WM (n=10), 2. chronic active rim (n=7) vs. control WM (n=10) 3. inactive rim (n=8) vs. control WM (n=10) 4. MS-PL-NAWM (n=15) vs. control WM (n=10)

Then, the initial analyses including log transformation, normalization, and statistical analysis were performed on the established comparisons using an online tool GEO2R on the NCBI platform, utilizing the GEOquery and limma packages. Subsequently, genes exhibiting

the most significant differential expression based on p-value and adjusted p-value were selected.

DEGs and pathway analysis

The processed expression data were imported into RStudio software for the following analysis. Genes associated with iron metabolism were identified and extracted using subset function. Subsequently, differential expression analysis was conducted to compare each pathological state with the control group. Genes with log2FC > 0.6 and p-value < 0.05 were considered significantly upregulated, while genes with log2FC < -0.6 and p-value < 0.05 were considered significantly downregulated. To visualize DEGs volcano plots were created using the ggplot2 package. Additionally, Venn diagrams were generated using the VennDiagram package to illustrate the overlap of DEGs across the different conditions. The pie charts were created to depict each group's alterations in iron metabolic pathways.

A complete list of genes involved in iron homeostasis, sourced from the RGD database (https://rgd.mcw.edu/rgdweb/pathway/pathwayRecord.html?acc_id=PW:0000590&species=Human#gviewer) specific to humans, along with their physiological functions and their presence or absence in the available dataset, is detailed in Table 1.

Table 1. List of genes involved in iron regulatory pathways and related information.

Symbol	Name	Pathway	Gene Ontology (molecular function)	Detection in dataset
ACO1	aconitase 1	iron homeostasis pathway	3 iron, 4 sulfur cluster binding [GO:0051538]; 4 iron, 4 sulfur cluster binding [GO:0051539]; aconitate hydratase activity [GO:0003994]; citrate dehydratase activity [GO:0047780]; iron-responsive element binding [GO:0030350]; metal ion binding [GO:0046872]; RNA binding [GO:0003723]	Detected
FBXL5	F-box and leucine rich repeat protein 5	iron homeostasis pathway	iron ion binding [GO:0005506]; ubiquitin-protein transferase activity [GO:0004842]	Detected
IREB2	iron responsive element binding protein 2	iron homeostasis pathway	4 iron, 4 sulfur cluster binding [GO:0051539]; aconitate hydratase activity [GO:0003994]; iron-responsive element binding [GO:0030350]; metal ion binding [GO:0046872]; RNA binding [GO:0003723]	Detected
NCOA4	nuclear receptor coactivator 4	iron homeostasis pathway	transcription coactivator activity [GO:0003713]	Detected
PCBP1	poly(rC) binding protein 1	iron homeostasis pathway	cadherin binding [GO:0045296]; DNA-binding transcription factor activity, RNA polymerase II-specific [GO:0000981]; mRNA binding [GO:0003729]; RNA binding [GO:0003723]; sequence-specific single stranded DNA binding [GO:0098847]; single-stranded DNA binding [GO:0003697]	Detected
PCBP2	poly(rC) binding protein 2	iron homeostasis pathway	C-rich single-stranded DNA binding [GO:1990829]; enzyme binding [GO:0019899]; mRNA binding [GO:0003729]; RNA binding [GO:0003723]; single-stranded DNA binding [GO:0003697]; ubiquitin protein ligase binding [GO:0031625]	Detected
PCBP3	poly(rC) binding protein 3	iron homeostasis pathway	C-rich single-stranded DNA binding [GO:1990829]; DNA-binding transcription repressor activity, RNA polymerase II-specific [GO:0001227]; double-stranded DNA binding [GO:0003690]; mRNA binding [GO:0003729]; RNA binding [GO:0003723]	Detected
PCBP4	poly(rC) binding protein 4	iron homeostasis pathway	DNA binding [GO:0003677]; mRNA 3'-UTR binding [GO:0003730]; mRNA binding [GO:0003729]; RNA binding [GO:0003723]	Detected
CIAO1	cytosolic iron-sulfur assembly component 1	cytosolic iron-sulfur cluster protein assembly pathway		Detected
CIAO2A	cytosolic iron-	cytosolic iron-	metal ion binding [GO:0046872]	Non-

	sulfur assembly component 2A	sulfur cluster protein assembly pathway		Detected
CIAO2B	cytosolic iron-sulfur assembly component 2B	cytosolic iron-sulfur cluster protein assembly pathway		Non-Detected
CIAO3	cytosolic iron-sulfur assembly component 3	cytosolic iron-sulfur cluster protein assembly pathway	4 iron, 4 sulfur cluster binding [GO:0051539]; metal ion binding [GO:0046872]	Non-Detected
CIAPIN1	cytokine-induced apoptosis inhibitor 1	cytosolic iron-sulfur cluster protein assembly pathway	2 iron, 2 sulfur cluster binding [GO:0051537]; 4 iron, 4 sulfur cluster binding [GO:0051539]; electron transfer activity [GO:0009055]; iron ion binding [GO:0005506]; methyltransferase activity [GO:0008168]	Detected
MMS19	MMS19 homolog, cytosolic iron-sulfur assembly component	cytosolic iron-sulfur cluster protein assembly pathway	enzyme binding [GO:0019899]; nuclear estrogen receptor binding [GO:0030331]; protein-macromolecule adaptor activity [GO:0030674]; signaling receptor complex adaptor activity [GO:0030159]; transcription coactivator activity [GO:0003713]	Detected
NDOR1	NADPH dependent diflavin oxidoreductase 1	cytosolic iron-sulfur cluster protein assembly pathway	electron transfer activity [GO:0009055]; FAD binding [GO:0071949]; flavin adenine dinucleotide binding [GO:0050660]; FMN binding [GO:0010181]; NADP binding [GO:0050661]; NADPH binding [GO:0070402]; NADPH-hemoprotein reductase activity [GO:0003958]; oxidoreductase activity [GO:0016491]; oxidoreductase activity, acting on iron-sulfur proteins as donors, NAD or NADP as acceptor [GO:0016731]; oxidoreductase activity, acting on NAD(P)H, heme protein as acceptor [GO:0016653]	Detected
NUBP1	NUBP iron-sulfur cluster assembly factor 1, cytosolic	cytosolic iron-sulfur cluster protein assembly pathway	4 iron, 4 sulfur cluster binding [GO:0051539]; ATP binding [GO:0005524]; ATP-dependent FeS chaperone activity [GO:0140663]; iron-sulfur cluster binding [GO:0051536]; metal ion binding [GO:0046872]; nucleotide binding [GO:0000166]	Detected
NUBP2	NUBP iron-sulfur cluster assembly factor 2, cytosolic	cytosolic iron-sulfur cluster protein assembly pathway	4 iron, 4 sulfur cluster binding [GO:0051539]; ATP binding [GO:0005524]; ATP-dependent FeS chaperone activity [GO:0140663]; iron-sulfur cluster binding [GO:0051536]; metal ion binding [GO:0046872]; nucleotide binding [GO:0000166]	Detected
ALAD	aminolevulinate dehydratase	heme biosynthetic pathway	catalytic activity [GO:0003824]; identical protein binding [GO:0042802]; porphobilinogen synthase activity [GO:0004655]; proteasome core complex binding [GO:1904854]; zinc ion binding [GO:0008270]	Detected
ALAS1	5´-aminolevulinate synthase 1	heme biosynthetic pathway	5-aminolevulinate synthase activity [GO:0003870]; identical protein binding [GO:0042802]; pyridoxal phosphate binding [GO:0030170]	Detected
ALAS2	5´-aminolevulinate synthase 2	heme biosynthetic pathway	5-aminolevulinate synthase activity [GO:0003870]; pyridoxal phosphate binding [GO:0030170]	Detected
CPOX	coproporphyrinogen oxidase	heme biosynthetic pathway	coproporphyrinogen oxidase activity [GO:0004109]; protein homodimerization activity [GO:0042803]; structural constituent of eye lens [GO:0005212]	Detected
FECH	Ferrochelatase	heme biosynthetic pathway	2 iron, 2 sulfur cluster binding [GO:0051537]; ferrochelatase activity [GO:0004325]; ferrous iron binding [GO:0008198]; heme binding [GO:0020037]; iron-responsive element binding [GO:0030350]; protein homodimerization activity [GO:0042803]	Detected
HMBS	hydroxymethylbilane synthase	heme biosynthetic pathway	hydroxymethylbilane synthase activity [GO:0004418]	Detected
PPOX	protoporphyrinogen oxidase	heme biosynthetic pathway	flavin adenine dinucleotide binding [GO:0050660]; oxygen-dependent protoporphyrinogen oxidase activity [GO:0004729]	Detected
SLC25A38	solute carrier family 25 member 38	heme biosynthetic pathway	glycine transmembrane transporter activity [GO:0015187]	Detected
TSPO	translocator protein	heme biosynthetic pathway	androgen binding [GO:0005497]; benzodiazepine receptor activity [GO:0008503]; cholesterol binding [GO:0015485]; cholesterol transfer	Detected

			activity [GO:0120020]; transmembrane transporter binding [GO:0044325]	
UROD	uroporphyrinogen decarboxylase	heme biosynthetic pathway	uroporphyrinogen decarboxylase activity [GO:0004853]	Detected
UROS	uroporphyrinogen III synthase	heme biosynthetic pathway	folic acid binding [GO:0005542]; uroporphyrinogen-III synthase activity [GO:0004852]	Detected
CP	ceruloplasmin	iron efflux pathway	copper ion binding [GO:0005507]; ferroxidase activity [GO:0004322]; oxidoreductase activity [GO:0016491]; protein-folding chaperone binding [GO:0051087]	Detected
HAMP	hepcidin antimicrobial peptide	iron efflux pathway	copper ion binding [GO:0005507]; hormone activity [GO:0005179]; iron ion transmembrane transporter inhibitor activity [GO:0097690]; signaling receptor binding [GO:0005102]	Detected
HEPH	hephaestin	iron efflux pathway	copper ion binding [GO:0005507]; ferrous iron binding [GO:0008198]; ferroxidase activity [GO:0004322]; oxidoreductase activity [GO:0016491]	Detected
SLC40A1	solute carrier family 40 member 1	iron efflux pathway	ferrous iron transmembrane transporter activity [GO:0015093]; identical protein binding [GO:0042802]; iron ion transmembrane transporter activity [GO:0005381]; metal ion binding [GO:0046872]; peptide hormone binding [GO:0017046]	Detected
FTH1	ferritin heavy chain 1	iron storage pathway	ferric iron binding [GO:0008199]; ferrous iron binding [GO:0008198]; ferroxidase activity [GO:0004322]; identical protein binding [GO:0042802]; iron ion binding [GO:0005506]; iron ion sequestering activity [GO:0140315]	Detected
FTL	ferritin light chain	iron storage pathway	ferric iron binding [GO:0008199]; ferrous iron binding [GO:0008198]; identical protein binding [GO:0042802]; iron ion binding [GO:0005506]	Detected
FTMT	ferritin mitochondrial	iron storage pathway	ferric iron binding [GO:0008199]; ferrous iron binding [GO:0008198]; ferroxidase activity [GO:0004322]; iron ion binding [GO:0005506]	Detected
PCBP1	poly(rC) binding protein 1	iron storage pathway	cadherin binding [GO:0045296]; DNA-binding transcription factor activity, RNA polymerase II-specific [GO:0000981]; mRNA binding [GO:0003729]; RNA binding [GO:0003723]; sequence-specific single stranded DNA binding [GO:0098847]; single-stranded DNA binding [GO:0003697]	Detected
PCBP2	poly(rC) binding protein 2	iron storage pathway	C-rich single-stranded DNA binding [GO:1990829]; enzyme binding [GO:0019899]; mRNA binding [GO:0003729]; RNA binding [GO:0003723]; single-stranded DNA binding [GO:0003697]; ubiquitin protein ligase binding [GO:0031625]	Detected
CYBRD1	cytochrome b reductase 1	iron uptake pathway	identical protein binding [GO:0042802]; metal ion binding [GO:0046872]; oxidoreductase activity [GO:0016491]; oxidoreductase activity, acting on metal ions [GO:0016722]; transmembrane ascorbate ferrireductase activity [GO:0140571]; transmembrane monodehydroascorbate reductase activity [GO:0140575]	Detected
PRNP	prion protein	iron uptake pathway	amyloid-beta binding [GO:0001540]; aspartic-type endopeptidase inhibitor activity [GO:0019828]; ATP-dependent protein binding [GO:0043008]; copper ion binding [GO:0005507]; cupric ion binding [GO:1903135]; cuprous ion binding [GO:1903136]; glycosaminoglycan binding [GO:0005539]; identical protein binding [GO:0042802]; lamin binding [GO:0005521]; microtubule binding [GO:0008017]; molecular adaptor activity [GO:0060090]; molecular condensate scaffold activity [GO:0140693]; molecular function activator activity [GO:0140677]; protease binding [GO:0002020]; protein sequestering activity [GO:0140311]; protein-containing complex binding [GO:0044877]; protein-folding chaperone binding [GO:0051087]; signaling receptor activity [GO:0038023]; transmembrane transporter binding [GO:0044325]; tubulin binding [GO:0015631]; type 5 metabotropic glutamate receptor binding [GO:0031802]	Detected
SLC11A2	solute carrier family 11 member 2	iron uptake pathway	cadmium ion binding [GO:0046870]; cadmium ion transmembrane transporter activity [GO:0015086]; cobalt ion transmembrane transporter activity [GO:0015087]; copper ion transmembrane transporter activity [GO:0005375]; ferrous iron transmembrane transporter activity [GO:0015093]; inorganic cation transmembrane transporter activity [GO:0022890]; iron ion transmembrane transporter activity [GO:0005381]; lead ion transmembrane transporter activity [GO:0015094]; manganese ion transmembrane transporter activity	Detected

			[GO:0005384]; nickel cation transmembrane transporter activity [GO:0015099]; retromer complex binding [GO:1905394]; solute:proton symporter activity [GO:0015295]; transition metal ion transmembrane transporter activity [GO:0046915]; vanadium ion transmembrane transporter activity [GO:0015100]; zinc ion transmembrane transporter activity [GO:0005385]	
SLC25A28	solute carrier family 25 member 28	iron uptake pathway	ferrous iron transmembrane transporter activity [GO:0015093]	Detected
SLC25A37	solute carrier family 25 member 37	iron uptake pathway	ferrous iron transmembrane transporter activity [GO:0015093]	Detected
SLC39A14	solute carrier family 39 member 14	iron uptake pathway	cadmium ion transmembrane transporter activity [GO:0015086]; ferrous iron transmembrane transporter activity [GO:0015093]; iron ion transmembrane transporter activity [GO:0005381]; manganese ion transmembrane transporter activity [GO:0005384]; monoatomic anion:monoatomic cation symporter activity [GO:0015296]; monoatomic cation:bicarbonate symporter activity [GO:0140410]; zinc ion transmembrane transporter activity [GO:0005385]	Detected
SLC39A8	solute carrier family 39 member 8	iron uptake pathway	monoatomic cation:bicarbonate symporter activity [GO:0140410]; zinc ion transmembrane transporter activity [GO:0005385]; zinc:bicarbonate symporter activity [GO:0140412]	Detected
STEAP3	STEAP3 metalloreductase	iron uptake pathway	cupric reductase activity [GO:0008823]; ferric-chelate reductase (NADPH) activity [GO:0052851]; identical protein binding [GO:0042802]; metal ion binding [GO:0046872]; oxidoreductase activity, acting on metal ions, NAD or NADP as acceptor [GO:0016723]	Detected
TF	transferrin	iron uptake pathway	ferric iron binding [GO:0008199]; ferrous iron binding [GO:0008198]; iron chaperone activity [GO:0034986]; transferrin receptor binding [GO:1990459]	Detected
TFRC	transferrin receptor	iron uptake pathway	double-stranded RNA binding [GO:0003725]; Hsp70 protein binding [GO:0030544]; identical protein binding [GO:0042802]; protein homodimerization activity [GO:0042803]; protein kinase binding [GO:0019901]; protein-containing complex binding [GO:0044877]; RNA binding [GO:0003723]; transferrin receptor activity [GO:0004998]; virus receptor activity [GO:0001618]	Detected
ABCB7	ATP binding cassette subfamily B member 7	mitochondrial iron-sulfur cluster export pathway	ABC-type iron-sulfur cluster transporter activity [GO:0140481]; ATP binding [GO:0005524]; ATP hydrolysis activity [GO:0016887]; ATPase-coupled transmembrane transporter activity [GO:0042626]; heme transmembrane transporter activity [GO:0015232]; protein homodimerization activity [GO:0042803]	Detected
GFER	growth factor, augmenter of liver regeneration	mitochondrial iron-sulfur cluster export pathway	flavin adenine dinucleotide binding [GO:0050660]; flavin-linked sulfhydryl oxidase activity [GO:0016971]; growth factor activity [GO:0008083]; protein-disulfide reductase activity [GO:0015035]	Detected
BOLA3	bolA family member 3	mitochondrial iron-sulfur cluster protein biogenesis pathway	cell redox homeostasis [GO:0045454]; iron-sulfur cluster assembly [GO:0016226]; protein maturation by [4Fe-4S] cluster transfer [GO:0106035]	Detected
FDX1	ferredoxin 1	mitochondrial iron-sulfur cluster protein biogenesis pathway	2 iron, 2 sulfur cluster binding [GO:0051537]; electron transfer activity [GO:0009055]; iron ion binding [GO:0005506]	Detected
FDX2	ferredoxin 2	mitochondrial iron-sulfur cluster protein biogenesis pathway	2 iron, 2 sulfur cluster binding [GO:0051537]; electron transfer activity [GO:0009055]; metal ion binding [GO:0046872]	Non-Detected
FDXR	ferredoxin reductase	mitochondrial iron-sulfur cluster protein biogenesis pathway	ferredoxin-NADP+ reductase activity [GO:0004324]; NADPH-adrenodoxin reductase activity [GO:0015039]	Detected
GLRX5	glutaredoxin 5	mitochondrial iron-sulfur cluster	2 iron, 2 sulfur cluster binding [GO:0051537]; metal ion binding [GO:0046872]	Detected

		protein biogenesis pathway		
HSCB	HscB mitochondrial iron-sulfur cluster cochaperone	mitochondrial iron-sulfur cluster protein biogenesis pathway	ATPase activator activity [GO:0001671]; identical protein binding [GO:0042802]; metal ion binding [GO:0046872]; protein-folding chaperone binding [GO:0051087]	Detected
HSPA9	heat shock protein family A (Hsp70) member 9	mitochondrial iron-sulfur cluster protein biogenesis pathway	ATP binding [GO:0005524]; ATP hydrolysis activity [GO:0016887]; ATP-dependent protein folding chaperone [GO:0140662]; heat shock protein binding [GO:0031072]; protein folding chaperone [GO:0044183]; RNA binding [GO:0003723]; ubiquitin protein ligase binding [GO:0031625]; unfolded protein binding [GO:0051082]	Detected
IBA57	iron-sulfur cluster assembly factor IBA57	mitochondrial iron-sulfur cluster protein biogenesis pathway	RNA binding [GO:0003723]; transferase activity [GO:0016740]	Detected
ISCA1	iron-sulfur cluster assembly 1	mitochondrial iron-sulfur cluster protein biogenesis pathway	2 iron, 2 sulfur cluster binding [GO:0051537]; metal ion binding [GO:0046872]	Detected
ISCA2	iron-sulfur cluster assembly 2	mitochondrial iron-sulfur cluster protein biogenesis pathway	2 iron, 2 sulfur cluster binding [GO:0051537]; 4 iron, 4 sulfur cluster binding [GO:0051539]; identical protein binding [GO:0042802]; iron ion binding [GO:0005506]	Detected
ISCU	iron-sulfur cluster assembly enzyme	mitochondrial iron-sulfur cluster protein biogenesis pathway	2 iron, 2 sulfur cluster binding [GO:0051537]; ferrous iron binding [GO:0008198]; iron ion binding [GO:0005506]; molecular adaptor activity [GO:0060090]; protein homodimerization activity [GO:0042803]; zinc ion binding [GO:0008270]	Detected
LYRM4	LYR motif containing 4	mitochondrial iron-sulfur cluster protein biogenesis pathway	protein homodimerization activity [GO:0042803]	Detected
NFS1	NFS1 cysteine desulfurase	mitochondrial iron-sulfur cluster protein biogenesis pathway	cysteine desulfurase activity [GO:0031071]; iron-sulfur cluster binding [GO:0051536]; metal ion binding [GO:0046872]; protein homodimerization activity [GO:0042803]; pyridoxal phosphate binding [GO:0030170]	Detected
NFU1	NFU1 iron-sulfur cluster scaffold	mitochondrial iron-sulfur cluster protein biogenesis pathway	4 iron, 4 sulfur cluster binding [GO:0051539]; iron ion binding [GO:0005506]	Detected
NUBPL	NUBP iron-sulfur cluster assembly factor, mitochondrial	mitochondrial iron-sulfur cluster protein biogenesis pathway	4 iron, 4 sulfur cluster binding [GO:0051539]; ATP binding [GO:0005524]; ATP-dependent FeS chaperone activity [GO:0140663]; metal ion binding [GO:0046872]	Detected

RESULTS

Identifying Differentially Expressed Genes Involved in Iron Metabolism through MS Regions

By reanalyzing the microarray MS dataset, we identified 58 out of 62 genes involved in iron metabolism. Among these, 13 genes showed altered expression in MS lesion rims, while 12 genes were differentially expressed in the PL-NAWM compared to the control white matter (WM). Furthermore, the gene expression changes related to iron metabolism in the chronic active and inactive rims were separately compared to control WM. The most significant changes were observed in 15 genes showing altered expression in the rim of chronic active lesions (Fig. 1A). To identify gene expression changes specific to each lesion and common between MS lesions, each area (including all MS lesions, the chronic active rim, the inactive rim, and the PL-NAWM) was compared against the control WM (Fig. 1B). It was found that 6 of genes (*CP*, *CYBRD1*, *STEAP3*, *SLC39A14*,

ABCB7, *FTL*) were commonly upregulated among MS regions. In comparison, 4 genes (*PCBP4*, *NDOR1*, *FTH1*, *ALAD*) showed a common decrease in expression across these regions. Conversely, the number of genes specifically altered in each area was much lower. It included the genes *TSPO* (involved in heme biosynthesis) and *SLC39A8* (encodes one of the iron transporters into cells), whose expressions were specifically increased in the chronic active and inactive lesions rim, respectively. In addition, 2 genes, *TF* (transferrin, iron carrier) and *ALAS2* (involved in heme biosynthesis) were downregulated in the chronic active lesions rim, and the gene *PPOX* (also involved in heme biosynthesis) showed decreased expression in the MS peri-lesional normal-appearing white matter.

A

	RIM-MS-lesions	Chronic active rim	Inactive rim	MS-PL-NAWM
Total	13	15	12	12
Up	7	8	7	6
Down	6	7	5	6

B

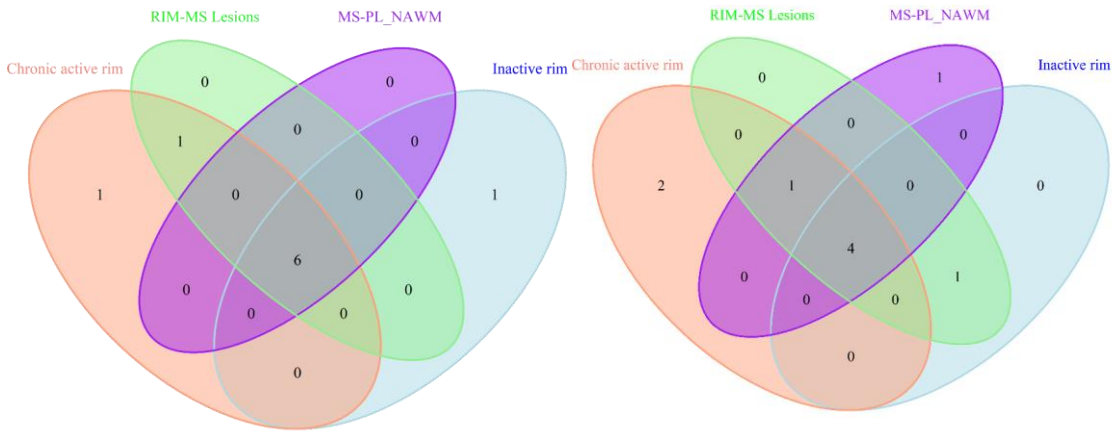

Fig. 1. The number of genes with changed expressing levels involved in iron metabolism in MS lesions and the PL-NAWM. A - The Venn diagram represents the number of overlapping and lesion-specific DEGs between MS lesion types (chronic active and inactive rim) and PL-NAWM compared to control WM tissues. B - The number of altered genes in each MS lesion and the PL-NAWM is reported.

Differentially Expressed Genes Involved in Iron Metabolism at the MS Lesions Rim

In the next step, we analyzed significant alterations in the genes related to iron homeostasis at the rim of MS lesions V.S control WM based on p-values. The expression of key iron-regulating genes, responsible for iron uptake, storage, and export, has been significantly altered. The genes *CP* (ceruloplasmin; ferroxidase that helps iron export from cells), *FTL* (ferritin light chain), *STEAP3* (endosomal ferrireductase involved in

iron uptake), *SLC40A1* (FPN, iron exporter), *CYBRD1* (plasma membrane iron reductase; effective in iron entry into cells), *ABCB7* (involved in the transfer of cytosolic iron-sulfur clusters from mitochondria to cytosol), *SLC39A14* (ZIP14; one of the iron uptake transporters), showed significant increase in expression. On the other hand, in this region, genes *PCBP4* (involved in iron homeostasis), *TFRC* (transferrin receptor, responsible for iron entry into cells), *NDOR1* (NADPH-dependent reductase; involved in cytosolic iron-sulfur cluster protein assembly pathway), *NUBP2* (essential for maturation of extramitochondrial Fe-S proteins), *ALAD* (catalyzes the second step in the porphyrin and heme biosynthetic pathway), and *FTH1* (ferritin heavy chain), showed a significant decrease in expression compared to the control WM (Fig. 2A, B).

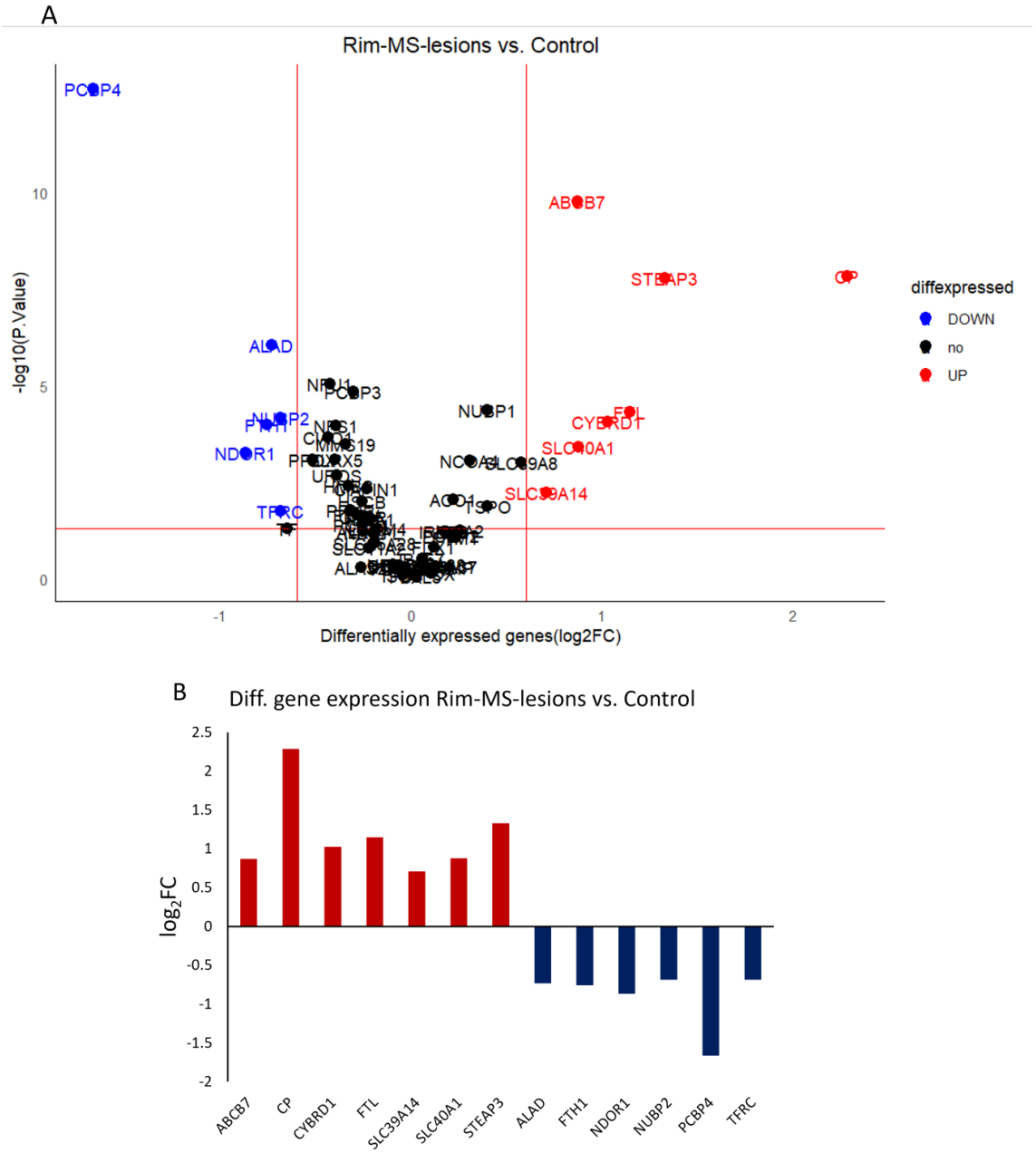

Fig. 2. Differentially expressed genes involved in iron regulatory pathways in the rim of MS lesions. A - The volcano plot illustrates DEGs in the rim of MS lesions compared to the control WM. Genes with decreased expression were plotted in blue, and genes with increased expression were plotted in red. B - The bar chart represents genes with increased expression (red) and decreased expression (blue) in the rim of MS lesions compared to control WM based on log2 fold change (Log2FC>0.6 / <-0.6, p-Value <0.05).

Differentially Expressed Genes Involved in Iron Metabolism at the Chronic Active Rim

In the chronic active rim as compared to the control white matter (WM), a notable upregulation was observed in the expression of genes such as *CP*, *FTL*, *STEAP3*, *SLC40A1*, *CYBRD1*, *ABCB7*, *SLC39A14*, and *TSPO* (involved in heme biosynthesis). Conversely, a significant downregulation was noted in the expression of genes including *PCBP4*, *TF* (transferrin, an iron carrier), *NDOR1*, *NUBP2*, *ALAS2*, *ALAD* (involved in the production of essential enzymes for heme synthesis), and *FTH1* (Fig. 3A, B).

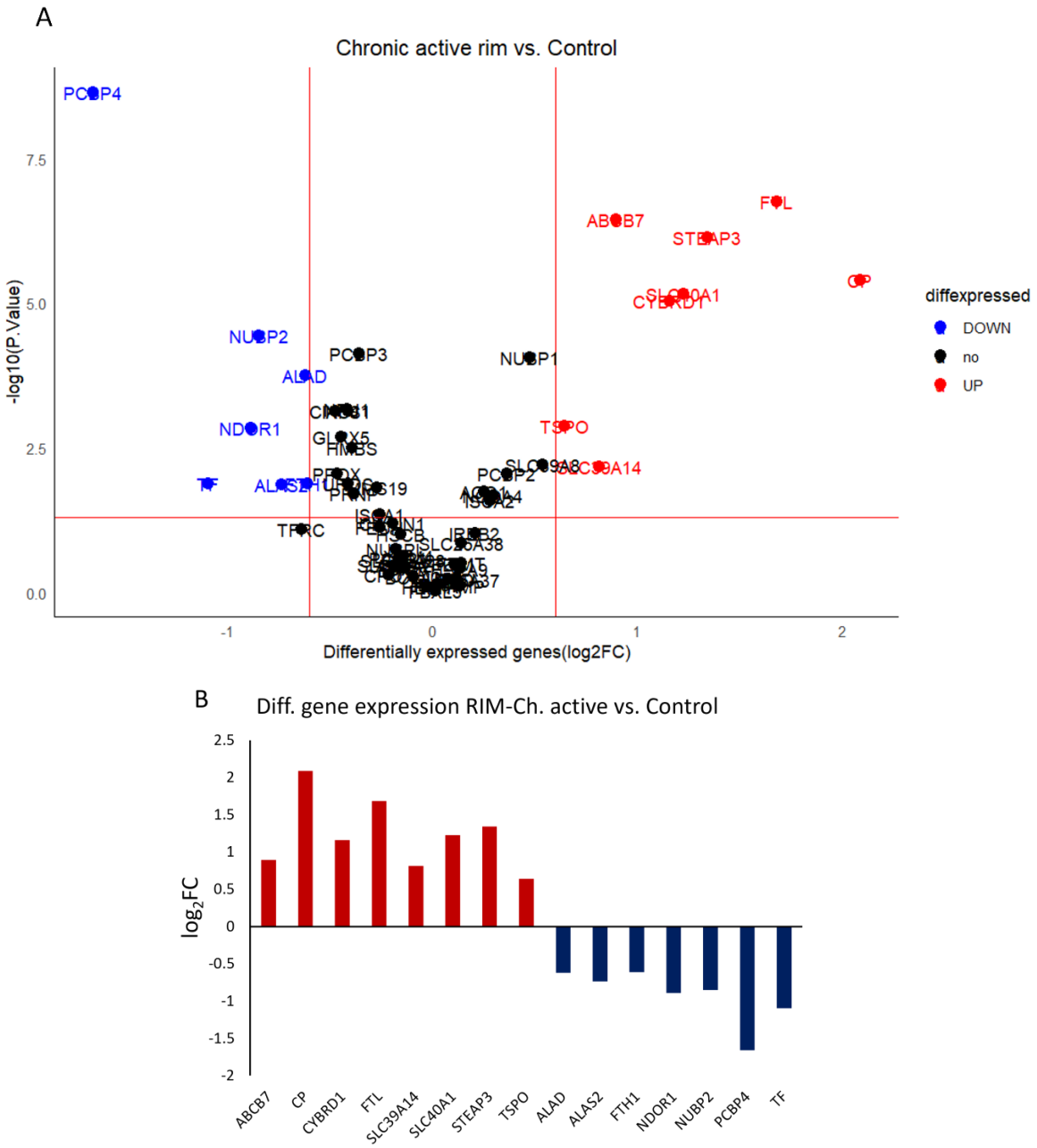

Fig. 3. Differentially expressed genes involved in iron regulatory pathways in the chronic active lesion rim. A - The volcano plot illustrates DEGs in the chronic active rim compared to the control WM. Genes with decreased expression were plotted in blue, and genes with increased expression were plotted in red. B - The bar chart represents genes with increased expression (red) and decreased expression (blue) in the chronic active rim compared to control WM based on log2 Fold Change (Log2FC > 0.6 / < -0.6, P-Value < 0.05).

Differentially Expressed Genes Involved in Iron Metabolism at the Inactive Rim

The analysis of DEGs between the inactive rim and the control white matter (WM) reveals notable changes in gene expression. Genes such as *CP*, *STEAP3*, *ABCB7*, *CYBRD1*, *FTL*, *SLC39A14*, *and SLC39A8* (ZIP8, an iron transporter into cells) have shown a significant increase in expression. Conversely, genes *PCBP4*, *FTH1*, *ALAD*, *NDOR1*, *NUBP2*, and *TFRC* demonstrated a substantial decrease in expression (Fig. 4A, B).

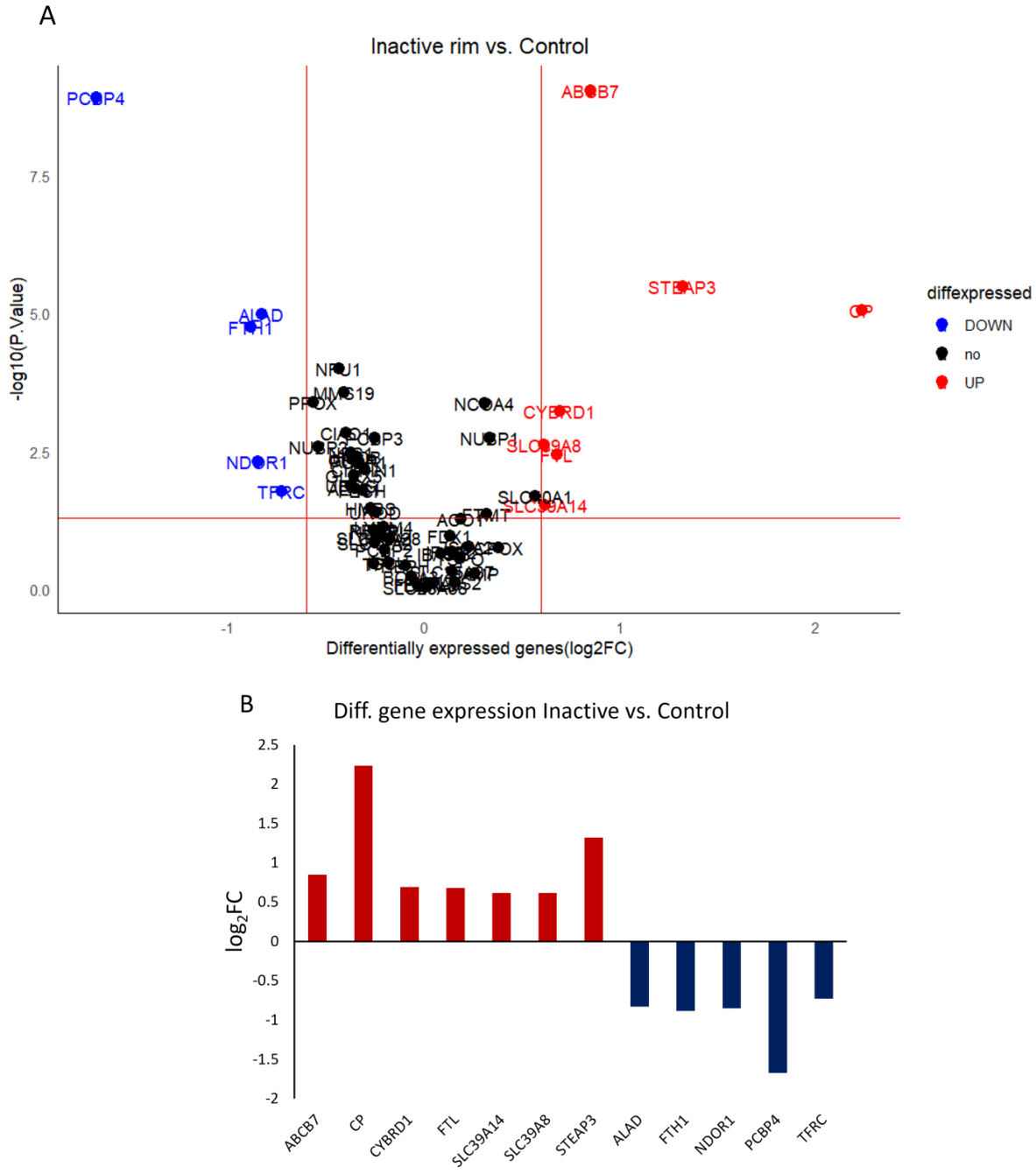

Fig. 4. Differentially expressed genes involved in iron regulatory pathways in the inactive rim. A - The volcano plot illustrates DEGs in the inactive rim compared to the control WM. Genes with decreased expression were plotted in blue, and genes with increased expression were plotted in red. B - The bar chart represents genes with increased expression (red) and decreased expression (blue) in the inactive rim compared to control WM based on log2 Fold Change (Log2FC > 0.6 / < -0.6, P-Value < 0.05).

Differentially Expressed Genes Involved in Iron Metabolism at the PL-NAWM

Eventually, we investigated the genes with altered expression in the PL-NAWM compared to the control WM. Despite the lack of myelin destruction and axonal damage in these areas, the genes encoding key iron-regulatory factors still exhibited significant changes in expression; Specifically, the upregulation was observed in the genes *CP*, *CYBRD1*, *STEAP3*, *ABCB7*, *SLC39A14*, *and FTL*, while significant downregulation was noted in the genes *PCBP4*, *NDOR1*, *NUBP2*, *ALAD*, *FTH1*, and *PPOX* (Fig. 5A, B).

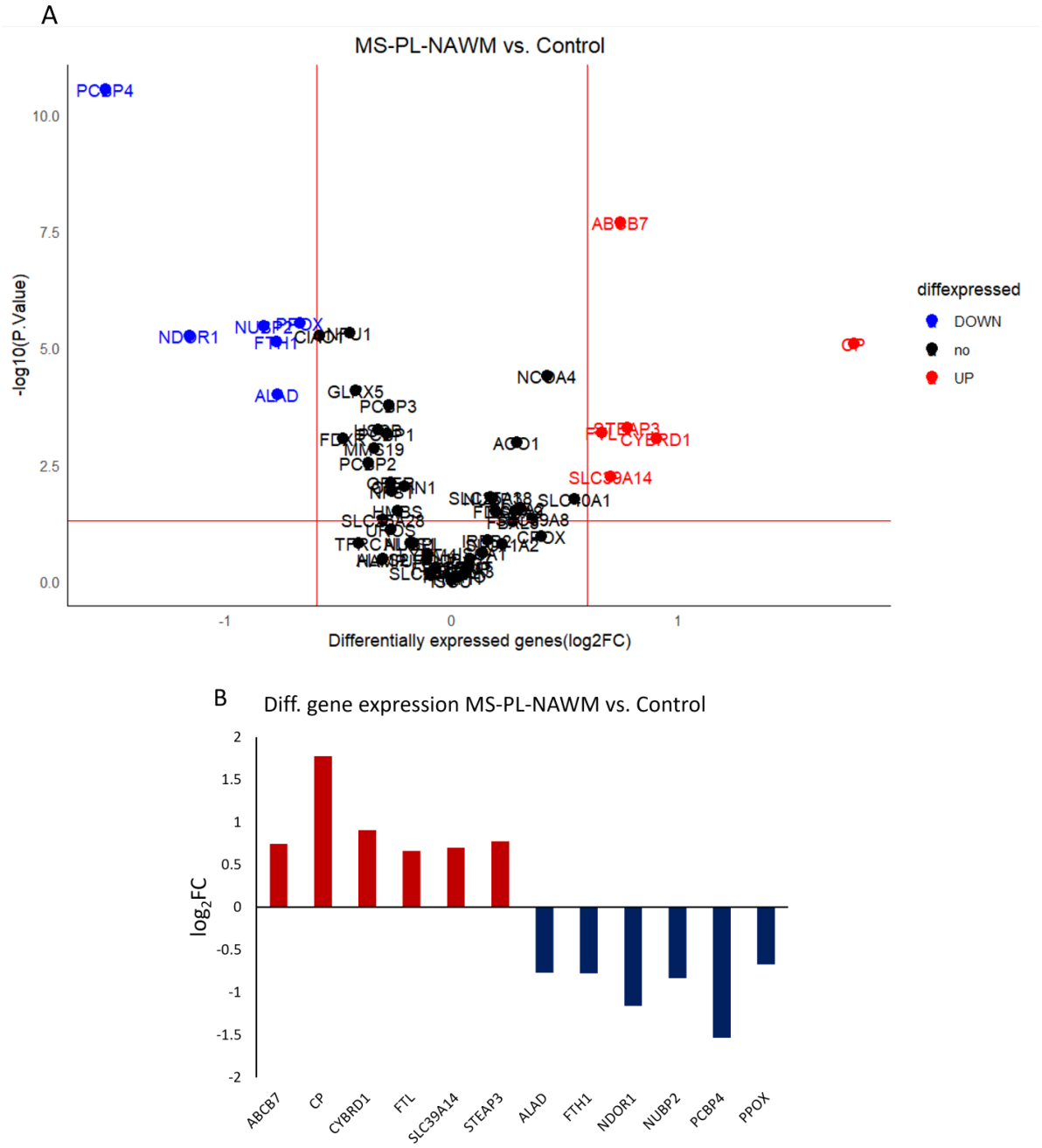

Fig. 5. Differentially expressed genes involved in iron regulatory pathways in the MS-PL-NAWM. A - The volcano plot illustrates DEGs in the MS-PL-NAWM compared to the control WM. Genes with decreased expression were plotted in blue, and genes with increased expression were plotted in red. B - The bar chart represents genes with increased expression (red) and decreased expression (blue) in the MS-PL-NAWM compared to control WM based on log2 Fold Change (Log2FC > 0.6 / < -0.6, P-Value < 0.05).

Investigating the changes in iron regulatory pathways in various types of MS lesions and PL-NAWM

Given the significant changes observed in the expression of genes encoding factors that play a crucial role in iron regulation and homeostasis within all types of MS lesions and the PL-NAWM, we decided to investigate how these genes contribute to changes in iron regulatory pathways, particularly within each distinct region. Pathway analysis of DEGs revealed significant alterations in the iron uptake, iron efflux, iron storage pathway, iron homeostasis, heme biosynthetic, cytosolic iron-sulfur cluster protein assembly, and mitochondrial iron-sulfur cluster export pathways (Fig. 6).

These findings indicate a notable prevalence of significant changes and the highest number of DEGs associated with the iron uptake pathway in various MS lesions and the PL-NAWM. Specifically, the chronic active rim exhibits a 27% prevalence, the inactive rim 42%, all MS lesions collectively 31%, and the PL-NAWM 25%. Furthermore, the chronic active rim's most significant changes are linked to the heme synthesis pathway (20%), while the inactive rim is associated with the iron storage pathway (17%). The changes in MS lesions' rim are equally distributed among three pathways involved in iron storage and export, and cytosolic iron-sulfur cluster protein assembly (15%). Similarly, the PL-NAWM exhibits equal distribution among three pathways related to iron storage, biosynthesis of heme, and cytosolic iron-sulfur cluster protein assembly (17%).

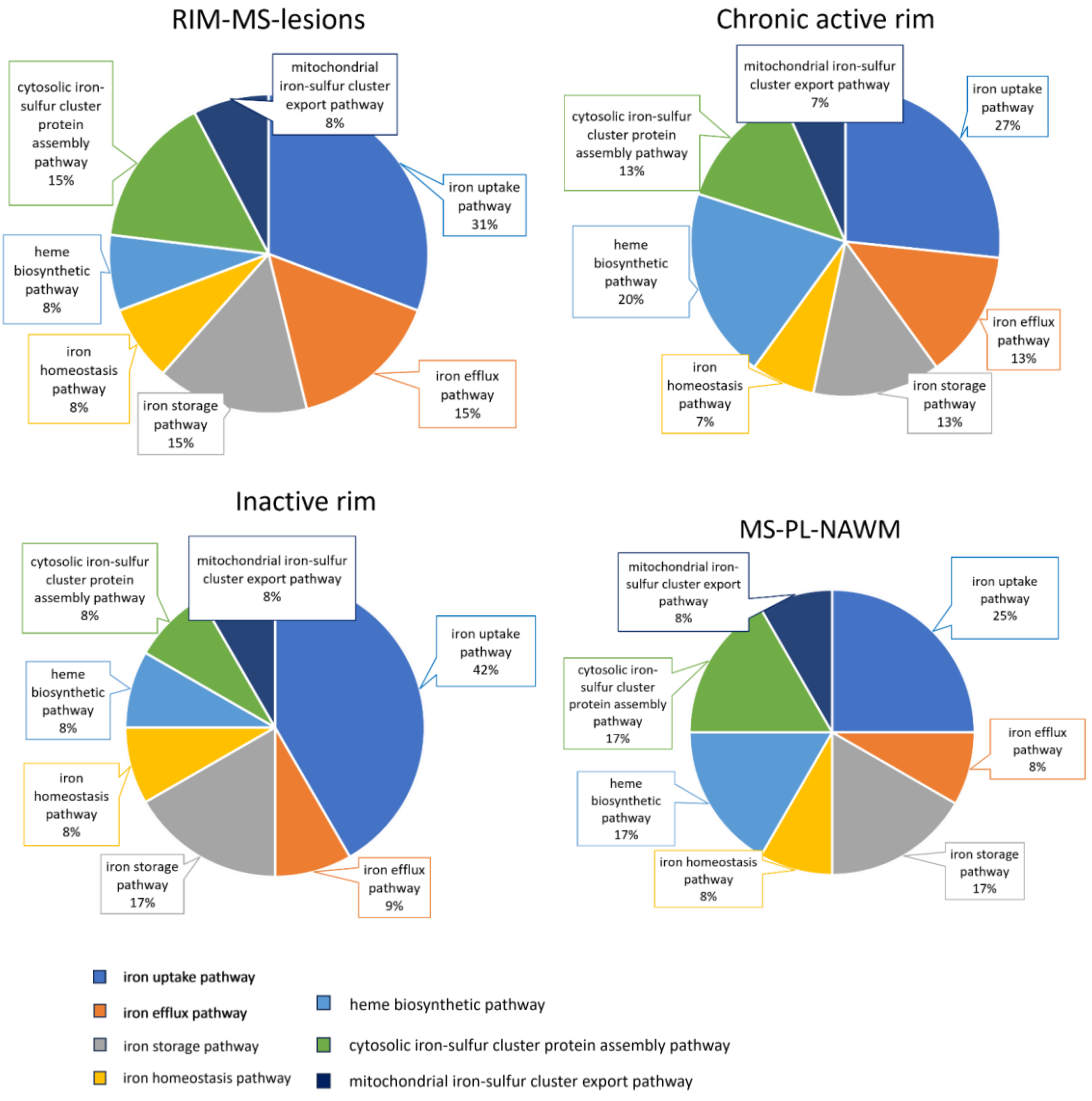

Fig. 6. Changes in DEGs-associated iron regulatory pathways in different MS lesion types and PL-NAWM. The pie chart represents the percentage of changes related to each iron regulatory pathway in MS lesions and PL-NAWM compared to the control WM.

DISCUSSION

In the present study, by reanalyzing DEGs from the microarray MS human dataset we provide the transcriptional profile of genes involved in iron metabolism through lesions and peri-lesional NAWM in patients with MS. These findings effectively indicate the significant alterations in the iron regulatory pathways in both chronic active and inactive rims and also in the PL-NAWM of MS patients. The most alterations were related to the iron uptake pathway, which showed more activity (Fig. 6). Along with our study, a single-cell RNA sequencing (sc-RNAseq) study performed on the microglia isolated from post-mortem gray matter (GM) and WM tissues, mentioned significant changes in iron metabolism in the GM's microglia (23). In detail, we reported the key iron regulatory genes differentially expressed across all four pathologically distinct regions. These results are particularly noteworthy due to the significant alterations observed in genes associated with iron regulatory pathways in PL-NAWM (Fig 5). These changes are also evident in various MS lesions (Figs 2-4). Notably, these genetic modifications precede plaque formation and may be causally linked to the genesis of lesions and the progression of MS pathology. ZIP14 (SLC39A14) and ZIP8 (SLC39A8) are members of the divalent metal transporter family responsible for transporting ferrous iron into cells (24, 25). CYBRD1 is an enzyme located on the plasma membrane acting as a ferric reductase (26). It forms a complex with divalent metal transporters on the plasma membrane, facilitating the iron entry into the cell by converting extracellular ferric to ferrous iron. The upregulation of *SLC39A14* and *CYBRD1* genes has been consistently observed in all MS lesions and the PL-NAWM (Fig 2-5), which may lead to higher levels of ferrous iron, the toxic and unstable form of iron, inside the cells. Moreover, the STEAP3 protein, an endosomal metalloreductase, is implicated in iron uptake through the transferrin-dependent pathway by converting ferric to ferrous iron within endosomes (27). The increased expression of the *STEAP3* gene detected in all lesions and the PL-NAWM (Fig 2-5) likely contributes to elevated labile iron levels within the cells. On the other hand, the expression of the ferritin light chain (*FTL*) gene, responsible for the ferritin complex formation to store iron in a non-toxic, ferric form, has increased (Fig 2-5). The snRNA-seq study, conducted on various types of MS lesions also demonstrated substantial upregulation of the ferritin genes (*FTL* and *FTH1*) in activated glial cells at the chronic active edge lesion (28). Moreover, another snRNA-seq in MS normal-appearing prefrontal cortices has revealed an upregulation of these genes in oligodendrocytes and *FTH1* in astrocytes (29). In contrast to these findings and other expression studies on MS animal models (13, 14), the expression of the ferritin heavy chain (*FTH1*) gene has notably decreased in these areas (Fig 2-5). The presence of this protein is essential not only for the ferritin complex formation but also as a ferroxidase to catalyze the conversion of ferrous to ferric iron to facilitate the storage of iron within the ferritin core (5). Consequently, despite the increased amounts of labile iron, it seems that the iron storage pathway has been disrupted, impeding the assembly of the ferritin complex for safely acquiring and storing excess iron within the cells. As a result, reactive ferrous iron may have built up inside the cells.

We have also noted an upregulation in the expression of ceruloplasmin (*CP*) ferroxidase (Fig 2-5), which plays a key role in converting iron from its ferrous to ferric state at the plasma membrane, thereby facilitating the iron efflux from the cells (30). Additionally, at the chronic active rim, a notable upregulation in the ferroportin (*SLC40A1*) gene expression, along with an increased expression of the *CP* has been observed (Fig 3). This finding contradicts previous studies indicating a decrease in ferroportin at the protein level in neurons and glial cells, likely due to hepcidin-mediated degradation (12-14). The heightened ferroportin expression observed at the transcriptional level suggests a compensatory mechanism. Just as in the RNAseq study on PBMC samples taken from the blood of SPMS patients, an increase in the expression of the *SLC40A1* gene has been reported (31). Moreover, there has been a reduction in the transferrin (TF) gene expression in this specific area (Fig 3). TF, through its binding to ferric iron, plays a crucial

role in facilitating the appropriate allocation of iron among diverse cells while preventing the accumulation of reactive iron in the intercellular space. Consequently, the diminished expression of this protein suggests a potential increase in labile iron levels within the extracellular space.

In the inactive rim, there has been a notable downregulation in the expression of the transferrin receptor (*TFRC*), while the expression of the *SLC39A8* (ZIP8) has shown upregulation (Fig 4). This pattern indicates an augmented influx of iron into the cells, leading to elevated free and labile iron, with a decrease in storage capacity in ferritin proteins. Overall, both chronic active and inactive lesions rim, show a noticeable reduction in iron entry through the transferrin-dependent pathway. Conversely, there is a marked increase in the transferrin-independent pathways for iron entry into the cells.

Accordingly, our findings suggest notable changes in the iron regulatory gene expressions across the lesions and even in the PL-NAWM, which lead to dysregulation in iron homeostasis. This imbalance likely contributes to neurodegenerative processes associated with MS by promoting oxidative stress due to excess reactive iron, potentially exacerbating inflammation and neuronal damage (32, 33). The labile iron participates in the Fenton reaction, producing hydroxyl free radicals by reacting with hydrogen peroxide. In excessive labile iron status, the production of hydroxyl radicals increases which can lead to lipid peroxidation, DNA damage, mitochondrial dysfunction, and eventually oxidative stress (34). This may be triggering ferroptosis which has a crucial role in promoting MS pathology (35).

Notably, the observed modifications in the PL-NAWM can be regarded as early indicators of MS pathology, potentially resulting in iron accumulation within the cells or intercellular space. This accumulation may contribute to the lesion initiation, propagation, and subsequent damage. Recognizing these molecular changes holds promise for facilitating timely MS diagnosis. Furthermore, the genes exhibiting modified expression patterns in the MS lesions may be regarded as potential targets for developing therapeutic interventions.

Considering the varied expression of iron regulatory genes within nerve cells based on their specific functions, it is crucial to investigate the individual cells within MS lesions using the available snRNA-seq data. This targeted approach is essential for obtaining a more precise and insightful analysis.

ACKNOWLEDGEMENTS

This article is part of the dissertation entitled "Investigating the effect of deferiprone on microglia phenotypes in an animal model of optic nerve demyelination," which was done at Tarbiat Modares University. The authors sincerely appreciate Elham Parandavar and Paria Pooyan for their helpful guidance on data analysis techniques.

FUNDING INFORMATION

This study was supported by the Iran National Science Foundation (INSF) (grant number. 4004518).

CONFLICT OF INTEREST STATEMENT:

The authors declare no conflict of interest.

REFERENCES

[1] Todorich B, Pasquini JM, Garcia CI, Paez PM, Connor JR. Oligodendrocytes and myelination: the role of iron. Glia. 2009;57(5):467-78.

[2] Crichton RR, Dexter DT, Ward RJ. Brain iron metabolism and its perturbation in neurological diseases. Monatshefte für Chemie - Chemical Monthly. 2011;142(4):341-55.

[3] Jomova K, Valko M. Importance of Iron Chelation in Free Radical-Induced Oxidative Stress and Human. Curr Pharm Des. 2011;17(31):3460-73.

[4] Li J, Cao F, Yin HL, Huang ZJ, Lin ZT, Mao N, et al. Ferroptosis: past, present and future. Cell Death Dis. 2020;11(2):88.

[5] Cheli VT, Correale J, Paez PM, Pasquini JM. Iron Metabolism in Oligodendrocytes and Astrocytes, Implications for Myelination and Remyelination. ASN Neuro. 2020;12:1759091420962681.

[6] Rouault TA. Iron metabolism in the CNS: implications for neurodegenerative diseases. Nat Rev Neurosci. 2013;14(8):551-64.

[7] Wang J, Pantopoulos K. Regulation of cellular iron metabolism. Biochem J. 2011;434(3):365-81.

[8] LeVine SM. Iron deposits in multiple sclerosis and Alzheimer's disease brains. Brain Res. 1997;760(1-2):298–303.

[9] Weigel KJ, Lynch SG, LeVine SM. Iron chelation and multiple sclerosis. ASN Neuro. 2014;6(1):e00136.

[10] Hunter RL, Liu M, Choi DY, Cass WA, Bing G. Inflammation and age-related iron accumulation in F344 rats. Curr Aging Sci. 2008;1(2):112-21.

[11] Zivadinov R, Weinstock-Guttman B, Pirko I. Iron deposition and inflammation in multiple sclerosis. Which one comes first. BMC Neurosci. 2011;12(60).

[12] Urrutia P, Aguirre P, Esparza A, Tapia V, Mena NP, Arredondo M, et al. Inflammation alters the expression of DMT1, FPN1 and hepcidin, and it causes iron accumulation in central nervous system cells. J Neurochem. 2013;126(4):541-9.

[13] Zarruk JG, Berard JL, Passos dos Santos R, Kroner A, Lee J, Arosio P, et al. Expression of iron homeostasis proteins in the spinal cord in experimental autoimmune encephalomyelitis and their implications for iron accumulation. Neurobiol Dis. 2015;81:93-107.

[14] Lee NJ, Ha SK, Sati P, Absinta M, Nair G, Luciano NJ, et al. Potential role of iron in repair of inflammatory demyelinating lesions. J Clin Invest. 2019;129(10):4365-76.

[15] Hametner S, Wimmer I, Haider L, Pfeifenbring S, Bruck W, Lassmann H. Iron and neurodegeneration in the multiple sclerosis brain. Ann Neurol. 2013;74(6):848-61.

[16] Kroner A, Greenhalgh AD, Zarruk JG, Passos Dos Santos R, Gaestel M, David S. TNF and increased intracellular iron alter macrophage polarization to a detrimental M1 phenotype in the injured spinal cord. Neuron. 2014;83(5):1098-116.

[17] Schuh C, Wimmer I, Hametner S, Haider L, Van Dam AM, Liblau RS, et al. Oxidative tissue injury in multiple sclerosis is only partly reflected in experimental disease models. Acta Neuropathol. 2014;128(2):247-66.

[18] Haider L, Fischer MT, Frischer JM, Bauer J, Hoftberger R, Botond G, et al. Oxidative damage in multiple sclerosis lesions. Brain. 2011;134(Pt 7):1914-24.

[19] Fischer MT, Wimmer I, Hoftberger R, Gerlach S, Haider L, Zrzavy T, et al. Disease-specific molecular events in cortical multiple sclerosis lesions. Brain. 2013;136(Pt 6):1799-815.

[20] Bakshi R, Shaikh ZA, Janardhan V. MRI T2 shortening ('black T2') in multiple sclerosis: frequency, location, and clinical correlation. Neuroreport. 2000;11(1):15-21.

[21] Dal-Bianco A, Grabner G, Kronnerwetter C, Weber M, Hoftberger R, Berger T, et al. Slow expansion of multiple sclerosis iron rim lesions: pathology and 7 T magnetic resonance imaging. Acta Neuropathol. 2017;133(1):25-42.

[22] Hendrickx DAE, van Scheppingen J, van der Poel M, Bossers K, Schuurman KG, van Eden CG, et al. Gene Expression Profiling of Multiple Sclerosis Pathology Identifies Early Patterns of Demyelination Surrounding Chronic Active Lesions. Front Immunol. 2017;8:1810.

[23] van der Poel M, Ulas T, Mizee MR, Hsiao CC, Miedema SSM, Adelia, et al. Transcriptional profiling of human microglia reveals grey-white matter heterogeneity and multiple sclerosis-associated changes. Nat Commun. 2019;10(1):1139.

[24] Wang CY, Jenkitkasemwong S, Duarte S, Sparkman BK, Shawki A, Mackenzie B, et al. ZIP8 is an iron and zinc transporter whose cell-surface expression is up-regulated by cellular iron loading. J Biol Chem. 2012;287(41):34032-43.

[25] Liuzzi JP, Aydemir F, Nam H, Knutson MD, Cousins RJ. Zip14 (Slc39a14) mediates non-transferrin-bound iron uptake into cells. Proc Natl Acad Sci U S A. 2006;103(37):13612-7.

[26] Oakhill JS, Marritt SJ, Gareta EG, Cammack R, McKie AT. Functional characterization of human duodenal cytochrome b (Cybrd1): Redox properties in relation to iron and ascorbate metabolism. Biochim Biophys Acta. 2008;1777(3):260-8.

[27] Lambe T, Simpson RJ, Dawson S, Bouriez-Jones T, Crockford TL, Lepherd M, et al. Identification of a Steap3 endosomal targeting motif essential for normal iron metabolism. Blood. 2009;113(8):1805-8.

[28] Absinta M, Maric D, Gharagozloo M, Garton T, Smith MD, Jin J, et al. A lymphocyte-microglia-astrocyte axis in chronic active multiple sclerosis. Nature. 2021;597(7878):709-14.

[29] Kihara Y, Zhu Y, Jonnalagadda D, Romanow W, Palmer C, Siddoway B, et al. Single-Nucleus RNA-seq of Normal-Appearing Brain Regions in Relapsing-Remitting vs. Secondary Progressive Multiple Sclerosis: Implications for the Efficacy of Fingolimod. Front Cell Neurosci. 2022;16:918041.

[30] Patel BN, Dunn RJ, Jeong SY, Zhu Q, Julien JP, David S. Ceruloplasmin regulates iron levels in the CNS and prevents free radical injury. J Neurosci. 2002;22(15):6578-86.

[31] Stojkovic L, Jovanovic I, Dincic E, Djordjevic A, Kuveljic J, Djuric T, et al. Targeted RNAseq Revealed the Gene Expression Signature of Ferroptosis-Related Processes Associated with Disease Severity in Patients with Multiple Sclerosis. Int J Mol Sci. 2024;25(5).

[32] Ferreira KPZ, Oliveira SR, Kallaur AP, Kaimen-Maciel DR, Lozovoy MAB, de Almeida ERD, et al. Disease progression and oxidative stress are associated with higher serum ferritin levels in patients with multiple sclerosis. J Neurol Sci. 2017;373:236-41.

[33] Stephenson E, Nathoo N, Mahjoub Y, Dunn JF, Yong VW. Iron in multiple sclerosis: roles in neurodegeneration and repair. Nat Rev Neurol. 2014;10(8):459-68.

[34] Nunez MT, Urrutia P, Mena N, Aguirre P, Tapia V, Salazar J. Iron toxicity in neurodegeneration. Biometals. 2012;25(4):761-76.

[35] Viktorinova A, Durfinova M. Mini-Review: Is iron-mediated cell death (ferroptosis) an identical factor contributing to the pathogenesis of some neurodegenerative diseases? Neurosci Lett. 2021;745:135627.